Channel Sounding of Loaded Reverberation Chamber for Over-the-Air Testing of Wireless Devices—Coherence Bandwidth Versus Average Mode Bandwidth and Delay Spread

Xiaoming Chen, Per-Simon Kildal, *Fellow, IEEE*, Charlie Orlenius, and Jan Carlsson, *Member, IEEE*

***Abstract*—This letter finds the relation between different parameters that characterize the reverberation chamber as a channel emulator for over-the-air (OTA) testing of wireless devices and components. It is shown experimentally for the first time that the coherence bandwidth is proportional to the average mode bandwidth of the chamber. Both coherence bandwidth and average mode bandwidth increase when the chamber is loaded with absorbing objects, and thereby, the reverberation chamber can be controlled to emulate many different real-life environments. The relationship between RMS delay spread and coherence bandwidth are found from the measured channel response and are equal to the theoretical relation for isotropic multipath environments, being within previously published fundamental limits.**

***Index Terms*—Coherence bandwidth, delay spread, fading channel, mode bandwidth.**

I. Introduction

REVERBERATION chambers can be used for measuring over-the-air (OTA) performance of small antennas and wireless devices in multipath environments. The reverberation chamber is basically a metal cavity that is stirred to emulate a Rayleigh fading environment [1]. The chamber used in this letter makes use of platform stirring [2] and polarization stirring [3] to improve measurement accuracy. The measurements of antenna radiation efficiency, diversity gains, and capacity of multiple-input–multiple-output (MIMO) systems are explained in [4]. Reverberation chambers can also be used to measure total radiated power [5] and total isotropic sensitivity [6] of active wireless devices. For the sensitivity measurements, the delay spread and coherence bandwidth of the channels in the chamber may affect the results. Therefore, it is of importance to relate the emulated channels in the chamber to actual channels in different real-life environments. One of the purposes of this letter is to show to what extent the delay spread and coherence bandwidth can be controlled by loading the chamber with absorbing objects.

When the reverberation chamber is excited at a single frequency, modes resonant at neighboring frequencies will also be excited due to the finite Q-factor. The Q of a resonance is given by $f/\Delta f$, where f is the resonance frequency and Δf is the half-power (3-dB) bandwidth [7]. Thus, the mode bandwidth is defined as the frequency range over which the power in one excited mode is larger than half the power in the mode when it is excited at its resonance frequency. The modes are distributed over frequency. Therefore, it is convenient to use an average mode bandwidth Δf to determine the approximate number of excited modes by counting modes within Δf around the frequency of operation. This lends itself to using the average mode bandwidth of the chamber to control the number of excited modes in the chamber and, thereby, apparently the number of independent samples and, hence, the measurement accuracy. This letter will relate the mode bandwidth to the coherence bandwidth by measurements when the chamber is loaded to different amounts.

The Q-factor of a reverberation chamber was introduced in [8], and it was used to find an expression for the average power transfer function in the chambers. This expression becomes simpler and more easily interpretable when expressed in terms of average mode bandwidth $\delta f = f/Q$. This letter will show that average mode bandwidth holds even more advantages over Q-factor because it relates in simple ways to the coherence bandwidth commonly used to characterize real propagation channels in real-life multipath environments.

Coherence bandwidth is defined as the frequency range over which the channel is correlated. In real multipath environments, it is easier to measure RMS delay spreads than coherence bandwidths, which are inversely proportional quantities [9]. Therefore, RMS delay spread is more frequently used to characterize real multipath channels; see, e.g., the measured results for some indoor and outdoor environments in [9]–[13]. In this letter, measured RSM delay spreads with different loadings of the reverberation chamber are presented for comparison with those measured in real environments.

Manuscript received April 14, 2009. First published June 12, 2009; current version published July 21, 2009. This work was supported in part by the Swedish Governmental Agency for Innovation Systems (VINNOVA) within the VINN Excellence Center Chase and by the Swedish Foundation for Strategic Research (SSF) within the Strategic Research Center Charmant.

X. Chen and P.-S. Kildal are with the Antenna Group, Chalmers University of Technology, 412 96 Gothenburg, Sweden (e-mail: xiaoming.chen@chalmers.se, per-simon.kildal@chalmers.se).

C. Orlenius is with the Signals and Systems Group, Chalmers University of Technology, 412 96 Gothenburg, Sweden.

J. Carlsson is with the Electronics Group, Technical Research Institute of Sweden, 501 15 Boras, Sweden.

Color versions of one or more of the figures in this letter are available online at http://ieeexplore.ieee.org.

Digital Object Identifier 10.1109/LAWP.2009.2025149

II. Average Mode Bandwidth and Coherence Bandwidth in Reverberation Chamber

The introduction of average mode bandwidth Δf makes it possible to characterize all the different losses appearing in the reverberation chamber as additive contributions to Δf, i.e.,

$$\Delta f = \Delta f_{\mathrm{con}} + \Delta f_{\mathrm{obj}} + \Delta f_{\mathrm{ap}} + \Delta f_{\mathrm{ant}} \tag{1a}$$

$$\Delta f_{\mathrm{ant}} = \frac{\sum_{\mathrm{antennas}} c^3 e_{\mathrm{rad}}}{(16\pi^2 f^2 V)},$$

$$\Delta f_{\mathrm{obj}} = \frac{\sum_{\mathrm{objects}} c\sigma_{\mathrm{a}}}{(2\pi V)}. \tag{1b}$$

Equation (1a) is the same as (6) in [8], except that it is expressed in terms of $\Delta f = f/Q$ rather than Q. The different contributions to Δf are Δf_{con} due to finite wall conductivity, Δf_{obj} due to absorbing objects, Δf_{ap} due to aperture leakage contribution, and Δf_{ant} due to antennas inside the chamber. The detailed formulas for the two dominant contributions Δf_{ant} and Δf_{obj} are given in (1b), being given by [8, Equations (17) and (11)], where V is the volume of the chamber, e_{rad} the radiation efficiencies of the antennas, and σ_{a} the average absorption cross sections of the lossy objects, properly defined in [8].

Formulas (1a) and (1b) are useful in order to understand how Δf is or can be controlled. In practice, the average mode bandwidth Δf can be determined by using [8, Equation (44)] after having evaluated the average power transfer function G_{ch} between two antennas located inside the chamber. Using [8, Equation (44)] and $Q = f/\Delta f$ gives

$$\Delta f = \frac{c_0^3 e_{\mathrm{rad1}} e_{\mathrm{rad2}}}{(16\pi^2 f^2 V G_{\mathrm{ch}})} \tag{2}$$

where the factors e_{rad1} and e_{rad2} have been included in the formula in accordance with the mismatch factor in [8, Equation (16)]. e_{rad1} and e_{rad2} are the total radiation efficiencies of the two antennas as they will be observed in free-space, including their mismatch factors.

In reverberation chamber, the frequency response of the channel is a function of frequency and stirrer position, denoted as $H(f,n)$. This is the same as the S-parameter S_{21} measured between the ports of two antennas inside the reverberation chamber, which by power averaging over stirrer positions becomes G_{ch} in (2). The complex $R_f(\partial f)$ and envelope $\rho_f(\partial f)$ autocorrelation functions (ACFs) of the frequency response of the channel, as well as the theoretical relation between them [10], [14], are

$$R_f(\partial f) = \frac{E[H^*(f,n)\cdot H(f+\partial f,n)]}{E[|H(f,n)|^2]}$$

$$\rho_f(\partial f) = \frac{E[A(f,n)\cdot A(f+\partial f,n)]}{E[A(f,n)^2]} \tag{3}$$

$$A(f,n) = |H(f,n)| - E[|H(f,n)|]$$

$$\rho_f(\partial f) \approx |R_f(\partial f)|^2. \tag{4}$$

The expectations $E[\cdot]$ in these formulas are, in practice, often evaluated by integrating the product over a frequency band, but then we will not be able to see any possible frequency variations of the ACFs. Therefore, we have herein chosen to take the expectation over all the stirrer positions n in the reverberation chamber, each one corresponding to an independent realization of the channel. To gather so many channel realizations will be very time-consuming when performing measurements in real-life environments, but in the reverberation chamber, it is feasible. The coherence bandwidth B_{c} is in this letter defined as the frequency offset ∂f at which the complex correlation function is larger than 0.5, i.e., $R_f(B_{\mathrm{c}}) = 0.5$. Although this is the most common definition, other definitions also exist [10], [11], [13].

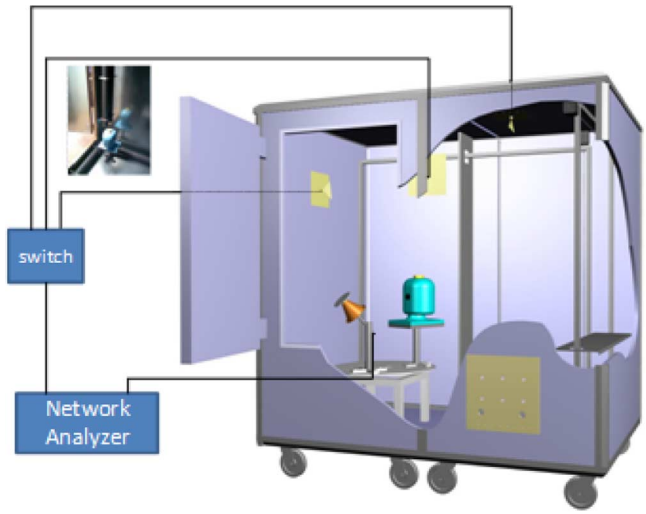

Fig. 1. Drawing of Bluetest reverberation chamber with two mechanical plate stirrers, one platform, and three wall antennas (The photograph inset in the upper left corner shows the head phantom and the location of the three absorber-filled PVC cylinders of load2 configuration).

When the reverberation chamber is excited at one frequency, modes at other frequencies around it will also be excited. Intuitively, modes within mode bandwidth are correlated, and the coherence bandwidth and mode bandwidth should be related. In order to verify this, the frequency responses of the chamber are measured using a vector network analyzer, when the chamber is loaded with different absorbing objects. The chamber used in this letter is the Bluetest HP reverberation chamber, with a size of 1.8 m × 1.7 m × 1.2 m (see Fig. 1). The mechanical stirring is performed by two metal plates that are moved stepwise. The platform stirring [2] is realized by a stepwise rotating platform upon which the antenna under test (AUT) is mounted, and polarization stirring [3] is achieved by three antennas mounted on three orthogonal walls. Average mode bandwidth and coherence bandwidth are calculated, according to (2) and (3), respectively. They are plotted in Fig. 2, where "empty" corresponds to unloaded chamber, "loading1" is a head phantom filled with brain-equivalent liquid, "loading2" is the head phantom plus three polyvinyl chloride (PVC) cylinders filled with microwave absorbers cut in small pieces, and "loading3" is the head phantom plus six such cylinders. The lossy cylinders were located along orthogonal corners of the chamber in such a way that they can be expected to load cavity modes of different polarizations equally

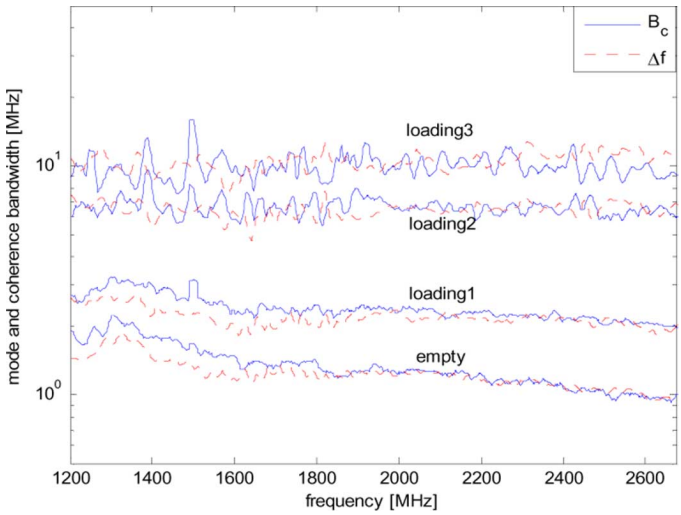

Fig. 2. Comparison of average mode bandwidths and coherence bandwidths ($B_{c,0.5}$; see Section III) for different loadings of the chamber.

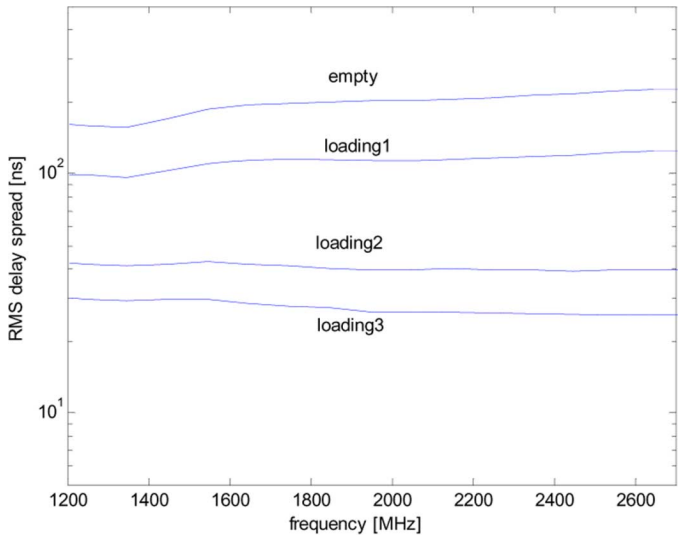

Fig. 3. RMS delay spread in reverberation chamber for the different loadings.

as much (TE and TM modes); see the photograph in the upper left corner of Fig. 1.

During one measurement, the platform is moved to 20 positions spaced by 18°, and for each platform position, the two stirrer-plates move simultaneously in a stepwise manner to 10 positions, each distributed evenly along the total distance they can move. The frequency sweep is done with a frequency step of 1 MHz. In order to improve the clearness of the graph in Fig. 2, all curves were smoothened over a 20-MHz moving window. Even after smoothening, both quantities show some irregular variation with frequency due to their statistical nature. Still, it is clearly seen that average mode bandwidth and coherence bandwidth are almost identical and frequency-invariant. The proportionality between coherence bandwidth and average mode bandwidth is important because it provides an easy way to determine the former via the latter. This proportionality was expected from previous theoretical publications [16], but this is the first time that it is verified by experiments. The empty chamber and chamber with head phantom show some frequency variations of the two bandwidths. The reason is that, for these two cases, the contribution to the chamber loading from the antennas are larger compared to the loading by the absorbing objects and the average mode bandwidth contribution due to antenna loading decay with frequency, whereas the average mode bandwidth contribution due to absorbing objects is almost invariant with frequency, all according to (1b).

The time-dispersive properties of multipath channels are usually characterized by their RMS delay spread. This can be computed from [9]

$$\sigma_\tau = \sqrt{\frac{\sum_k P(\tau_k)\tau_k^2}{\sum_k P(\tau_k)} - \left[\frac{\sum_k P(\tau_k)\tau_k}{\sum_k P(\tau_k)}\right]2}$$
$$P(\tau) = |h(\tau)|^2 \tag{5}$$

where the received power $P(\tau_k)$ at time delay τ_k is the so-called power delay spread (PDP), and $h(\tau)$ is the impulse response obtained from inverse fast Fourier transform (IFFT) of the channel frequency response $h(\tau, n) = \mathrm{IFFT}\{H(f, n)\}$ at each stirrer position n. RMS delay spread is calculated by (5) using PDP averaged over all the stirrer positions. Fig. 3 shows that the RMS delay spread can be reduced by increasing the loading of the chamber. The maximum RMS delay spread is around 200 ns. In principle, the Bluetest HP Reverberation Chamber can be used to emulate multipath channels with RMS delay spread down to around 20 ns and may be even a bit smaller with more loading. It is shown in [9] that the average RMS delay spreads is around 70–94 ns for indoor environments, 200–310 ns for suburban environments, and in the order of 1 μs for dense urban environments. This means that the reverberation chamber can emulate most channels in indoor environments and part of the channels in outdoor environments over the mobile radio communication frequency range.

III. Relationship Between RMS Delay Spread and Coherence Bandwidth in Reverberation Chamber

The inversely proportional relation between delay spread σ_τ and coherence bandwidth B_c can be expressed as

$$B_c = \frac{1}{(\kappa\sigma_\tau)} \tag{6}$$

where κ is a constant that depends on the environment, but also on how B_c is defined. B_c can be defined as the half-bandwidth (used in the present letter) or the full bandwidth, which is twice as large, and it can be defined as the bandwidth at which the complex correlation function has a value of 0.5, i.e., $R_f(B_c) = 0.5$ (used in the present letter, where the coherence bandwidth can be specifically denoted as $B_{c,0.5}$ with subscript 0.5 as the threshold), or at which the envelope correlation function has a value 0.5, i.e., $\rho_f(B_{\mathrm{env}}) = 0.5$. It has been shown in [14] both by measurements and theory that in reverberation chamber, $\kappa = 2\pi$ when the $\rho = 0.5$ half-bandwidth definition for B_{env} is used. This agrees well with the relationship obtained from the measurements in this letter. Theoretically, we have the following relation between the two abovementioned coherence bandwidths $B_c = \sqrt{3}B_{\mathrm{env}}$. Measurements have been done to determine the relationship between RMS delay spread

TABLE I
COMPARISONS OF DIFFERENT CONSTANTS κ RELATING DELAY SPREAD AND HALF-COHERENCE BANDWIDTHS IN (6) FOR THE TWO DIFFERENT DEFINITIONS OF THE LATTER

Case RC = Reverberation chamber	Half coherent bandwidth definition	
	Complex ACF $R_f(B_c) = 0.5$	Envelope ACF $\rho_f(B_{env}) = 0.5$
Real-life environments [13]	$1 < \kappa < 14$	$0.6 < \kappa < 8$
Theoretical for RC [14]	$\kappa = 2\sqrt{3}\pi$	$\kappa = 2\pi$
Measurements in RC [14]	$\kappa = 2\sqrt{3}\pi$	$\kappa = 2\pi$ with error less than 5%
Measurements in RC, present paper	$\kappa = 2\sqrt{3}\pi$	$\kappa = 2\pi$ with error less than 5%
Fundamental limit in [15]	$\kappa < 17.075$	$\kappa < 9.858$

and coherence bandwidth in real-life environments; see, e.g., [12] and [13]. In [13], their relationship is given as $1/(7\sigma_\tau) < 2B_{\mathrm{c},0.5} < 2/\sigma_\tau$. The above discussions of κ values are summarized in Table I, for the two half-bandwidth definitions of the coherence bandwidth. We see that the relation between coherence bandwidths and delay spread measured in reverberation chamber falls within the range of those determined by real-environment measurements. Besides, an inequality in [15] puts a fundamental limit on $B_{\mathrm{c},0.75}\sigma_\tau \geq 1/8.694$. This corresponds in our case to a fundamental limit on κ, which can be found by converting $B_{\mathrm{c},0.75}$ into $B_{\mathrm{c},0.75}$ to be

$$\kappa < 17.075. \tag{7}$$

As expected, the relation between coherence bandwidth and RMS delay spread obtained in the reverberation chamber also satisfies the fundamental limitation in (7).

IV. CONCLUSION

We have found experimentally that the average mode bandwidth Δf is proportional to the coherence bandwidth and is equal to it if the latter is properly defined. This was already claimed in [16], but with no experimental support. We have also shown that by loading the chamber, the channels in the reverberation chamber can be controlled to emulate most of the channels appearing in indoor environments and part of those appearing in outdoor quasi-static environments. Finally, the relationship between RMS delay spread and coherence bandwidth in reverberation chamber falls within the range of that determined by real-environment measurements.

REFERENCES

[1] P.-S. Kildal and K. Rosengren, "Correlation and capacity of MIMO systems and mutual coupling, radiation efficiency and diversity gain of their antennas: Simulations and measurements in reverberation chamber," *IEEE Commun. Mag.*, vol. 42, no. 12, pp. 102–112, Dec. 2004.

[2] K. Rosengren, P.-S. Kildal, C. Carlsson, and J. Carlsson, "Characterization of antennas for mobile and wireless terminals in reverberation chambers: Improved accuracy by platform stirring," *Microw. Opt. Technol. Lett.*, vol. 30, no. 20, pp. 391–397, Sep. 2001.

[3] P.-S. Kildal and C. Carlsson, "Detection of a polarization imbalance in reverberation chambers and how to remove it by polarization stirring when measuring antenna efficiencies," *Microw. Opt. Technol. Lett.*, vol. 32, no. 2, pp. 145–149, Jul. 2002.

[4] K. Rosengren and P.-S. Kildal, "Radiation efficiency, correlation, diversity gain and capacity of a six-monopole antenna array for a MIMO system: Theory, simulation and measurement in reverberation chamber," in *Proc. Microw. Antennas Propag.*, 2005, vol. 152, pp. 7–16.

[5] N. Serafimov, P.-S. Kildal, and T. Bolin, "Comparison between radiation efficiencies of phone antennas and radiated power of mobile phones measured in anechoic chambers and reverberation chamber," in *Proc. IEEE AP-S Int. Symp.*, San Antonio, TX, Jun. 2002, vol. 2, pp. 478–481.

[6] C. Orlenius, P.-S. Kildal, and G. Poilasne, "Measurement of total isotropic sensitivity and average fading sensitivity of CDMA phones in reverberation chamber," in *Proc. IEEE AP-S Int. Symp.*, Washington, DC, Jul. 2005, pp. 3–8.

[7] U. Carlberg, P.-S. Kildal, and J. Carlsson, "Study of antennas in reverberation chamber using method of moments with cavity green's function calculated by Ewald summation," *IEEE Trans. Electromagn. Compat.*, vol. 47, no. 4, pp. 805–814, Nov. 2005.

[8] D. A. Hill, M. T. Ma, A. R. Ondrejka, B. F. Riddle, M. L. Crawford, and R. T. Johnk, "Aperture excitation of electrically large, lossy cavities," *IEEE Trans. Electromagn. Compat.*, vol. 36, no. 3, pp. 169–178, Aug. 1994.

[9] T. S. Rappaport, *Wireless Communications-Principles and Practice*, 2nd ed. Upper Saddle River, NJ: Prentice-Hall, 2002, pp. 196–202.

[10] W. C. Jakes, *Microwave Mobile Communications*, 2nd ed. New York: Wiley, 1994, pp. 45–52.

[11] M. J. Gans, "A power-spectral theory of propagation in the mobile-radio environment," *IEEE Trans. Veh. Technol.*, vol. VT-21, no. 1, pp. 27–38, Feb. 1972.

[12] S. J. Howard, "Measurement and analysis of the indoor radio channel in frequency domain," *IEEE Trans. Instrum. Meas.*, vol. 39, no. 5, pp. 751–755, Oct. 1990.

[13] G. J. M. Janssen, P. A. Stigter, and R. Prasad, "Wideband indoor channel measurements and BER analysis of frequency selective multipath channels at 2.4, 4.75, and 11.5 GHz," *IEEE Trans. Commun.*, vol. 44, no. 10, pp. 1272–1288, Oct. 1996.

[14] X. Chen and P.-S. Kildal, "Theoretical derivation and measurements of the relationship between coherence bandwidth and RMS delay spread in reverberation chamber," in *Proc. 3rd Eur. Conf. Antenna Propag.*, Mar. 2009, pp. 23–27.

[15] B. H. Fleury, "An uncertainty relation for WSS processes and its application to WSSUS system," *IEEE Trans. Commun.*, vol. 44, no. 12, pp. 1632–1634, Dec. 1996.

[16] O. Delangre, P. De Doncker, M. Lienard, and P. Degauque, "Delay spread and coherence bandwidth in reverberation chamber," *Electron. Lett.*, vol. 44, no. 5, Feb. 2008.